catalysts

MDPI

Article

Hydroisomerisation and Hydrocracking of *n*-Heptane: Modelling and Optimisation Using a Hybrid Artificial Neural Network–Genetic Algorithm (ANN–GA)

Bashir Y. Al-Zaidi [1], Ali Al-Shathr [1], Amal K. Shehab [2], Zaidoon M. Shakor [1], Hasan Sh. Majdi [3], Adnan A. AbdulRazak [1,*] and James McGregor [4]

[1] Department of Chemical Engineering, University of Technology-Iraq, Baghdad 10066, Iraq; bashir.y.sherhan@uotechnology.edu.iq (B.Y.A.-Z.); ali.r.mohammedjawad@uotechnology.edu.iq (A.A.-S.); zaidoon.m.shakor@uotechnology.edu.iq (Z.M.S.)
[2] Ministry of Oil, Technical Directorate, Baghdad 00964, Iraq; amal.k.shehab@gmail.com
[3] Chemical Engineering and Oil Refinery Department, AlMustaqbal University College, Hilla 51001, Iraq; hasanshker1@gmail.com
[4] Department of Chemical and Biological Engineering, The University of Sheffield, Sir Robert Hadfield Building, Portobello Street, Sheffield S1 3JD, UK; james.mcgregor@sheffield.ac.uk
* Correspondence: adnan.a.alsalim@uotechnology.edu.iq

Abstract: In this paper, the focus is on upgrading the value of naphtha compounds represented by *n*-heptane (*n*-C_7H_{16}) with zero octane number using a commercial zeolite catalyst consisting of a mixture of 75% HY and 25% HZSM-5 loaded with different amounts, 0.25 to 1 wt.%, of platinum metal. Hydrocracking and hydroisomerisation processes are experimentally and theoretically studied in the temperature range of 300–400 °C and under various contact times. A feedforward artificial neural network (FFANN) based on two hidden layers was used for the purpose of process modelling. A total of 80% of the experimental results was used to train the artificial neural network, with the remaining results being used for evaluation and testing of the network. Tan-sigmoid and log-sigmoid transfer functions were used in the first and second hidden layers, respectively. The optimum number of neurons in hidden layers was determined depending on minimising the mean absolute error (MAE). The best ANN model, represented by the multilayer FFANN, had a 4–24–24–12 topology. The ANN model accurately simulates the process in which the correlation coefficient (R^2) was found to be 0.9918, 0.9492, and 0.9426 for training, validation, and testing, respectively, and an average of 0.9767 for all data. In addition, the operating conditions of the process were optimised using the genetic algorithm (GA) towards increasing the octane number of the products. MATLAB® Version 2020a was utilised to complete all required computations and predictions. Optimal operating conditions were found through the theoretical study: 0.85 wt.% Pt-metal loaded, 359.36 °C, 6.562 H_2/*n*-heptane feed ratio, and 3.409 h^{-1} weight-hourly space velocity (WHSV), through which the maximum octane number (*RON*) of 106.84 was obtained. Finally, those operating conditions largely matched what was calculated from the results of the experimental study, where the highest percentage of the resulting isomers was found with about 78.7 mol% on the surface of the catalyst loaded with 0.75 wt.% Pt-metal at 350 °C using a feed ratio of 6.5 H_2/*n*-C_7 and WHSV of 2.98 h^{-1}.

Keywords: *n*-heptane; Pt/HY-HZSM-5 zeolite catalyst; hydroisomrisation; hydrocracking; octane number; artificial neural network; optimisation; genetic algorithm

Citation: Al-Zaidi, B.Y.; Al-Shathr, A.; Shehab, A.K.; Shakor, Z.M.; Majdi, H.S.; AbdulRazak, A.A.; McGregor, J. Hydroisomerisation and Hydrocracking of *n*-Heptane: Modelling and Optimisation Using a Hybrid Artificial Neural Network–Genetic Algorithm (ANN–GA). *Catalysts* **2023**, *13*, 1125. https://doi.org/10.3390/catal13071125

Academic Editor: Javier Ereña

Received: 6 June 2023
Revised: 14 July 2023
Accepted: 14 July 2023
Published: 19 July 2023

1. Introduction

Gasoline is currently the main fuel for various means of transportation; it is a carcinogen if the resulting exhaust contains benzene in large quantities and it also constitutes a major problem in fuel production [1,2]. Accordingly, it is necessary to make naphtha fuel as free as possible from hydrocarbons such as alkanes and naphthenes, especially in the range from

hexane to heptane. Because naphtha contains large amounts of hydrocarbons in the n-C_6 and n-C_7 range, these compounds are considered the most prevalent precursors for the generation of harmful substances that are subsequently produced with the exhaust emitted from engines [3,4]. Hydroisomerisation and/or hydrocracking of the linear paraffins are essential processes to produce high-quality gasoline through converting the linear hydrocarbons with a low octane number, such as *n*-C_7 into branched hydrocarbons with a higher-octane number [5,6]. Branched paraffin does not contain olefin and aromatic components and has lower melting points and low sulphur content compared with that in the straight paraffins. Moreover, the efficiency of these processes depends on the reaction pathway, which is determined by the framework structure of the catalyst used and the reaction conditions [7]. Therefore, research continues in this field to choose the suitable commercial catalyst with the required specifications, optimal metal loading ratios, and accurate reaction conditions to reach an ideal catalytic reaction pathway for the linear hydrocarbon treatment process, and consequently raise the octane number of naphtha [8–10]. The type of catalyst utilised throughout the catalytic hydrotreating is a bifunctional catalyst (i.e., a noble metal support on an acid catalyst) [11]. Generally, metallic sites are required as a necessity for dehydrogenation/hydrogenation reactions; nevertheless, the acidic sites are essential to complete cracking/isomerisation reactions. Platinum metal has strong dehydrogenation and hydrogenation activities, while zeolite is used as an acid catalyst [12]. In fact, most zeolite catalysts are suitable for hydroisomerisation and/or hydrocracking because they have thermal stability; acidity and appropriate pore size do not hindrance the diffusion of their products from the zeolite opening pores, especially with zeolites that have multidimensional networks [13]. In the catalytic techniques of the chemical industries, heterogeneous reactions are used up to about 80%, and about 95% of them apply Y-type zeolites, especially in the petroleum industries [14]. The Y-type zeolite structure consists of a three-dimensional channel system and possess a large pore size, containing 12 tetrahedra with a maximum free pore diameter of Ø > 6.5 Å, while the ZSM-5-type zeolite structure consists of two intersection channels; one is straight and the other is sinusoidal and possesses a medium to small pore size, containing 10 tetrahedra with a maximum free pore diameter of 4.5 Å < Ø < 6.5 Å [15,16]. The ZSM-5 catalyst, due to its porous properties, is used to increase the selectivity of products as in the case of the fluidised bed reactor (i.e., FCC-unit) [17,18]. It was found in a study that the combination of HY zeolite and HZSM-23 zeolite together can significantly enhance the properties of isomerisation products [19]. On the other hand, developing an appropriate kinetic model based on the reaction mechanism is an important step in building a mathematical model. There are few investigations that have been interesting with regard to studying kinetic models of hydroisomerisation and hydrocracking reactions, such as Schweitzer et al. [20], who studied the kinetic model of *n*-heptane hydro-conversion using Pt/Beta catalyst, Song et al. [21], who investigated the kinetic model of the hydrocracking of vacuum gas oil using hydrotreating/hydrocracking catalysts, Vandegehuchte and his co-worker [22], who studied the kinetic model of *n*-hexadecane hydrocracking employing Pt/HBEA zeolite catalyst, Choudhury et al. [23], who explored the kinetic model of decane hydroisomerisation over Pt/HZSM-22 zeolite catalysts, and Martens et al. [24], who surveyed the kinetic model of *n*-octane to *n*-dodecane hydrocracking reaction over Pt/USY zeolite catalysts. Customarily, petroleum reactors comprise the reactions of cracking, polymerisation, dehydrogenation, alkylation, cyclisation, and isomerisation, which occur simultaneously [25]. Indeed, the hydrocracking reactions of alkenes take place at higher temperatures than the reactions of hydroisomerisation, and as a consequence the development of a reaction pathway describing hydroisomerisation and hydrocracking reactions of alkenes in industrial processes is very difficult [26]. In the past few years, modelling and simulation have become very necessary to keep pace with industry development through optimising the design of chemical units. Several models were suggested to predict and analyse production in terms of quality and quantity, and the results have shown a good improvement in most of these manufactures. Undeniably, the modelling is performed to understand the influence of process parameters such as temperature, pressure, volumetric flow rate,

weight hourly space velocity, metal loading, and the ratio of hydrogen atoms to carbon atoms (H/C) in hydrocarbon compounds [27,28]. Mathematical models are classified into two types, either empirical or deterministic models [29,30]. The empirical model, also named the statistical model, is based on prediction in contrast to deterministic models that rely on fundamental-principle calculations without relying on random interpretations. Artificial neural networks (ANNs) are evolutionary intelligence computational models, which are constricted by mathematical relations according to randomness correlations between input and output parameters [31,32]. The ANNs outperformed mathematical modelling in representing some chemical processes such as catalytic reactors [29]. ANNs can identify dependent and independent elements in nonlinear methods; however, black box is the main drawback of this method as it is strenuous to realize how the results were obtained. Nowadays, ANNs are employed to estimate the reaction performance for highly complex reactions such as hydroisomerisation and hydrocracking [4]. Furthermore, in systems of multiple input–output variables, ANNs have the ability to form relationships between these multiplexed variables. Estimation of the reaction rate without a kinetic model eliminates the errors arising from the selection of the kinetic model and the estimation of kinetic constants [33]. Traditional mathematical modelling can include algebraic, ordinary differential, and partial differential equations describing reaction temperature and reaction kinetics, while by using the ANN model, the effect of different factors, such as production cost (i.e., the effect of changing the composition of the feedstock on the distribution of products), calculating the cost of the technological regime (i.e., feasibility studies), the rate of catalyst deactivation (i.e., change of catalyst activity with reaction time), and the concentration of sulphur content, can be studied. Here, consideration should be given to the availability of sufficient experimental data showing the change in product distribution based on the change of these factors [29,34]. However, developing empirical models that render nonlinear relationships between products and reactants and cover the hydroisomerisation and hydrocracking reactions is an important task for the simulation, optimisation, and design of refinery reactors.

The aim of this study is to develop an artificial neural network model that can be easily used to simulate the performance of *n*-heptane hydrocracking and hydroisomerisation over a commercial bifunctional catalyst consisting of a mixture of HY and HZSM-5 zeolites. Previous studies have addressed the influence of only reaction parameters such as temperature and weight-per-hour space velocity (WHSV) on the product distribution and, thus, on the octane number (*RON*) of the product. In the current study, the effect of Pt-metal loading on the catalyst surface was added to the operating conditions as an effective variable. The efficiency of the developed empirical model was confirmed by the results obtained. The application of process optimisation was also made using the genetic algorithm approach to estimate the optimum operating conditions (e.g., wt.% Pt-metal loaded, reaction temperature, H_2/*n*-heptane feed ratio, and WHSV) that promise to increase the *RON* value of the reaction products. Finally, the optimal operating conditions obtained from the experimental results according to the highest molar percentage of the isomers produced on the catalyst surface were compared with the theoretical results calculated according to the artificial neural network model, to reach the degree of agreement between them and hence to determine the efficiency of the empirical model developed in this study.

2. Results and Discussion

2.1. Discussion of the Experimental Results

In the experimental aspect, the focus was on studying four important parameters in the hydroisomerisation and hydrocracking reactions, including WHSV, H_2/*n*-heptane feed ratio, wt.% Pt-metal loaded, and reaction temperature. Figure 1a–c shows the relationship of WHSV with selectivity towards the isomer generated on a catalyst surface. As mentioned earlier, the catalyst is formed from a mixture of 75 wt.% HY and 25 wt.% HZSM-5 and loaded with four different percentages of Pt-metal (i.e., 0.25, 0.5, 0.75, and 1 wt.%). The current study was conducted under temperatures ranging from 300 to 400 °C, as this range

of temperatures is the most common in the study of these types of catalytic reactions aimed at cracking hydrocarbons and increasing the production of isomers, and hence raising the value of the octane number of products. It is clearly observed that an increase in WHSV leads to a decrease in the percentage of isomers produced on the surface of the catalysts loaded with different amounts of Pt-metal. In fact, an increase in WHSV means a decrease in the contact time (i.e., catalyst weight/molar flow rate of n-C_7 in the feed, W/F) [35]. Therefore, it seems that the time spent by the reactants on the surface of the catalyst throughout the reaction is short and does not assist the catalytic hydroisomerisation reactions to occur at the level required to produce large quantities of isomers. In other words, a catalytic reaction is an interface phenomenon, and increasing the contact time between the active sites of the catalyst and the reactants can increase the reaction rate [36].

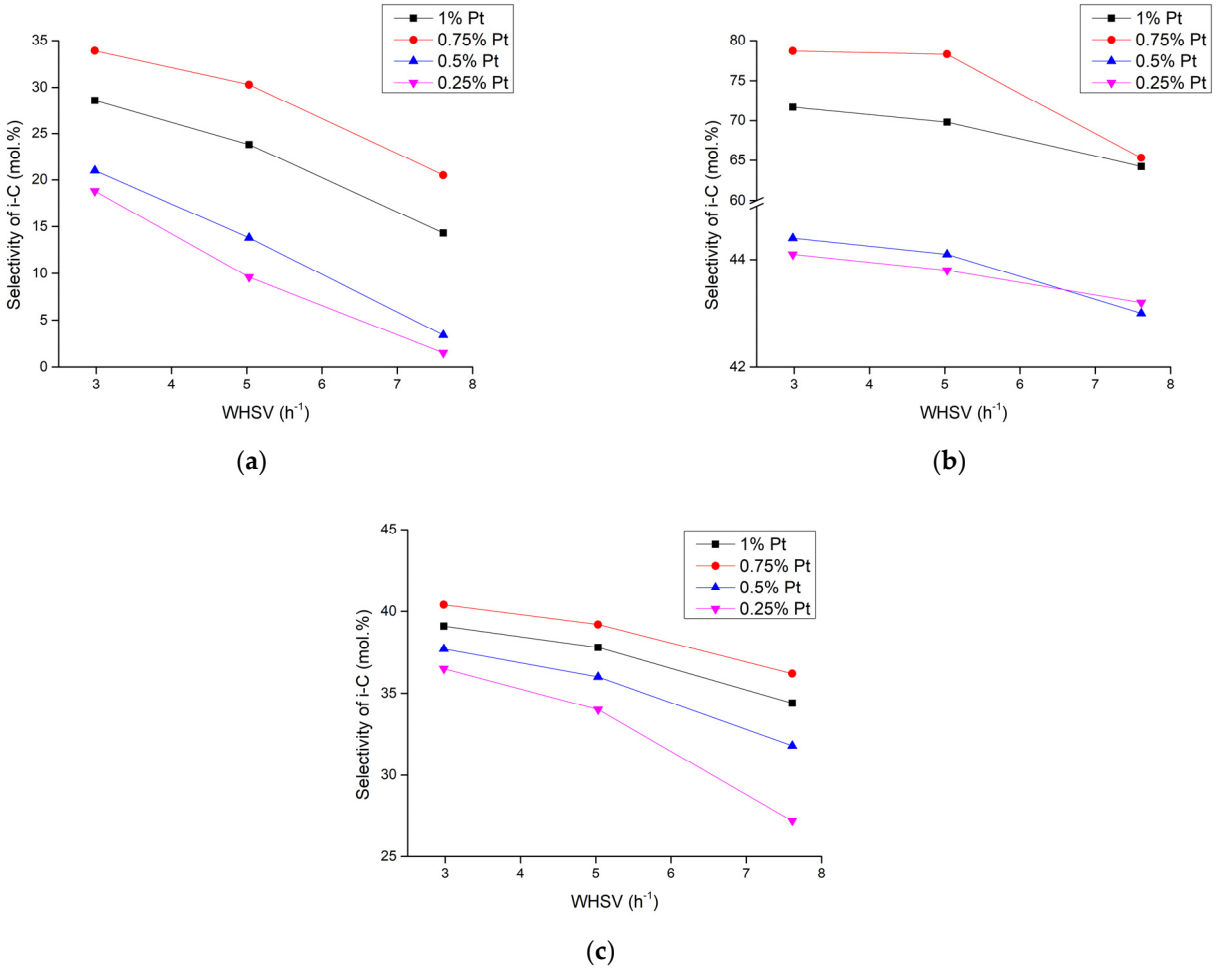

Figure 1. WHSV versus selectivity towards isomer production using different Pt-metal loading at (**a**) 300 °C, (**b**) 350 °C, and (**c**) 400 °C.

Likewise, the same catalytic behaviour is observed on the surface of bifunctional catalysts in Figure 2a–c, as increasing the H_2/n-heptane feed ratio leads to a decrease in the percentage of the produced isomers, whereas increasing the amount of excess hydrogen contributes to accelerating the hydrogenation/dehydrogenation reactions on the metal sites, which helps produce larger amounts of light gases with few carbon atoms such as C_1, C_2, and C_3 as well as pushes towards hydrocracking reactions instead of hydroisomerisation reactions [37]. Despite the differences in conclusions and discussions of results in the experimental study of both parameters, it can be noted that the catalytic behaviour is similar in terms of isomer production, whether using the WHSV in Figure 1 and/or the H_2/n-C_7 feed ratio in Figure 2, due to the fact that there is a direct relationship between them. Where the calculation of each WHSV value is based on the corresponding

contact time (W/F) value, this latter value is, in turn, dependent on the H_2/n-C_7 feed ratio value from which it was calculated. These parameters were studied experimentally for the purpose of using their results later in testing the efficiency of the empirical model developed in this study in its ability to predict and compare the theoretical results with the experimental results. Table 1 demonstrates the details of the laboratory-found results. In addition, the highest percentage of the resulting isomers of about 78.7 mol% was found on the catalyst surface loaded with 0.75 wt.% Pt-metal at 350 °C using a feed ratio of 6.5 H_2/n-C_7 and a WHSV of 2.98 h^{-1}, while the lowest percentage of the resulting isomers around 1.5 mol% was generated on the catalyst surface loaded with 0.25 wt.% Pt-metal at 300 °C using 10.5 H_2/n-C_7 feed ratio and 7.61 h^{-1} WHSV.

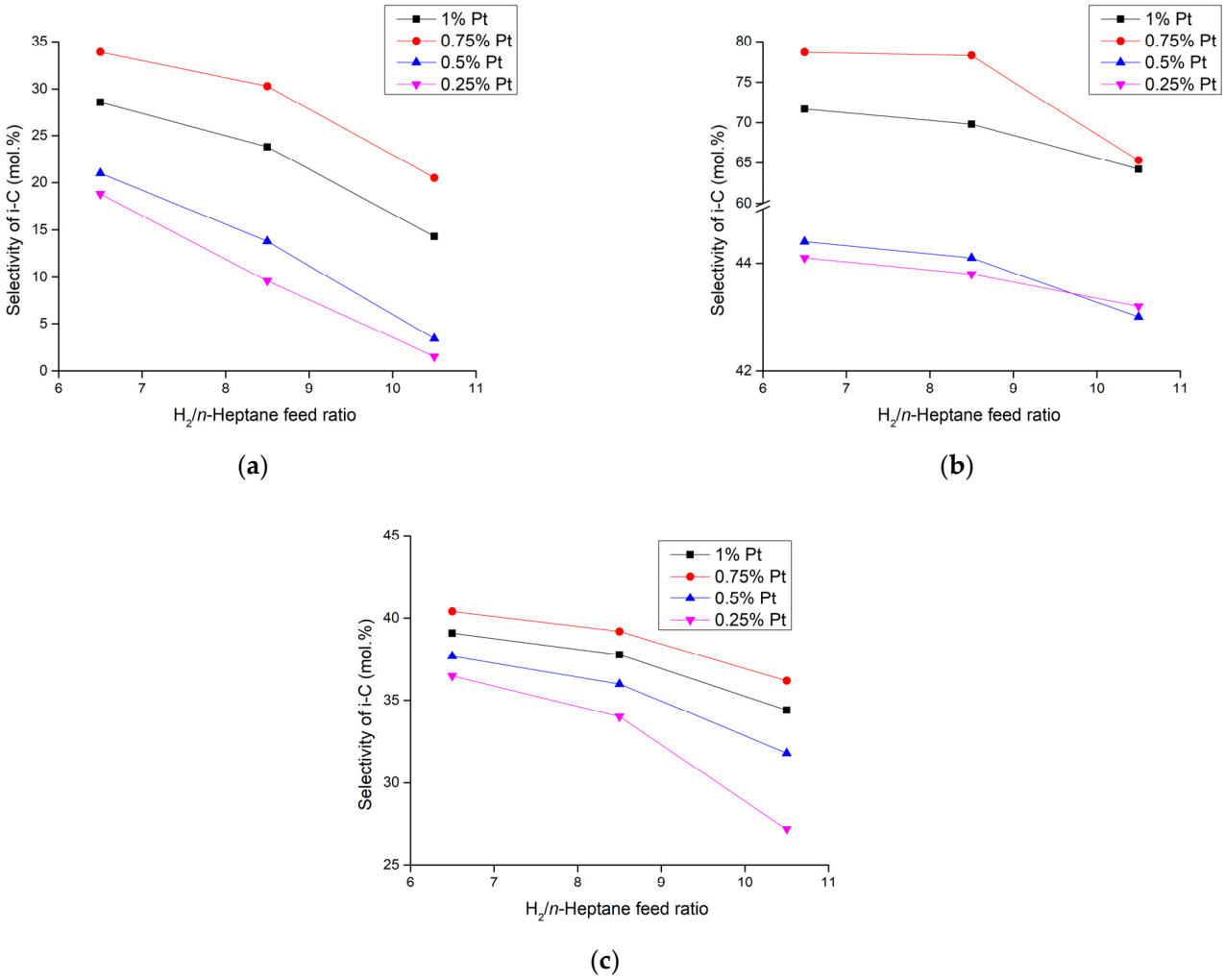

Figure 2. H_2/n-C_7 feed ratio versus selectivity towards isomer production using different Pt-metal loading at (**a**) 300 °C, (**b**) 350 °C, and (**c**) 400 °C.

Moreover, Figure 3a–c shows the results of 36 experiments that were performed to study the relationship between the percentages of Pt-metal loaded on the surface of a zeolite catalyst with the percentages of selectivity towards producing isomers at different reaction temperatures. The significant effect of the percentages of loaded metal on the catalytic behaviour of the catalysts throughout the hydroisomerisation/hydrocracking reaction can be seen in terms of the different percentages of the resulting isomers on their surfaces.

Table 1. Spectra of isomers produced on the surfaces of the catalysts loaded with different percentages of platinum.

Parameters			Selectivity towards Isomer Production (mol.%)			
Temperature (°C)	**H_2/*n*-C_7 Feed Ratio**	**WHSV (h^{-1})**	**0.25 wt.% Pt/HY-HZSM-5 Zeolite Catalyst**	**0.5 wt.% Pt/HY-HZSM-5 Zeolite Catalyst**	**0.75 wt.% Pt/HY-HZSM-5 Zeolite Catalyst**	**1 wt.% Pt/HY-HZSM-5 Zeolite Catalyst**
400	6.5	2.98	36.53	37.74	40.44	39.13
	8.5	5.03	34.04	36.01	39.18	37.79
	10.5	7.61	27.16	31.81	36.14	34.37
350	6.5	2.98	44.07	44.42	78.69	71.68
	8.5	5.03	43.75	44.11	78.3	69.85
	10.5	7.61	43.18	43.03	65.29	64.23
300	6.5	2.98	18.85	20.97	33.88	28.6
	8.5	5.03	9.63	13.82	30.26	23.81
	10.5	7.61	1.49	3.39	20.5	14.32

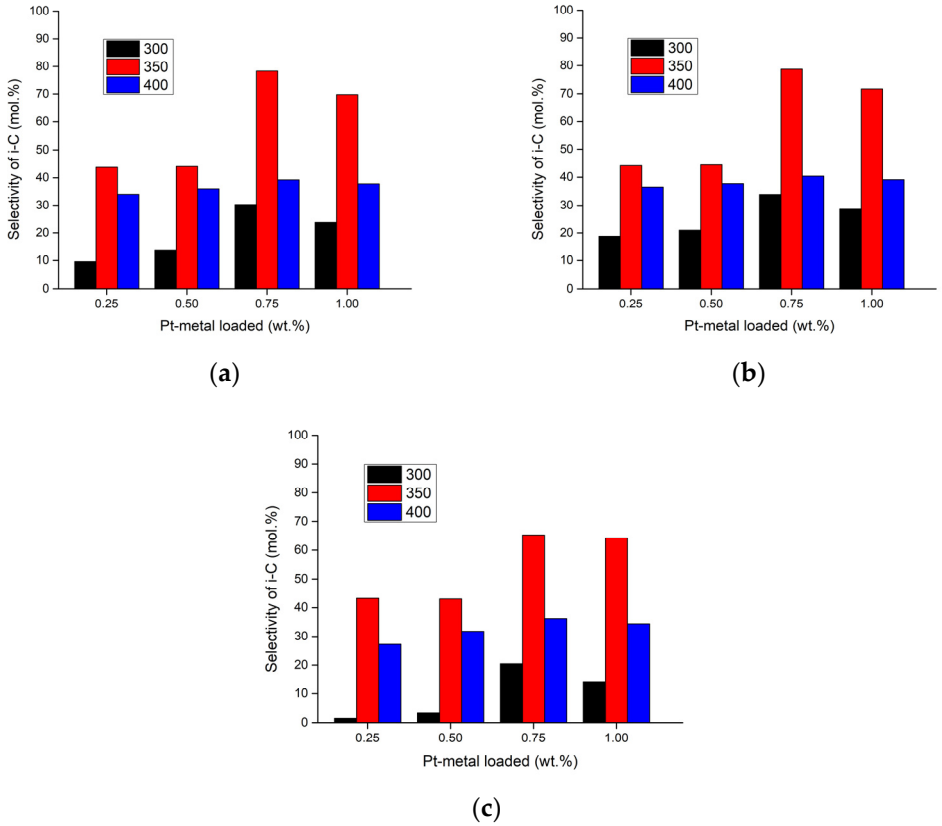

Figure 3. Pt-metal loading versus selectivity towards isomer production at 300, 350, and 400 °C using (**a**) WHSV = 2.98 h^{-1} and H_2/n-C_7 = 6.5, (**b**) WHSV = 5.03 h^{-1} and H_2/n-C_7 = 8.5, and (**c**) WHSV = 7.61 h^{-1} and H_2/n-C_7 = 10.5.

It can be seen that the percentage of production of isomers did not change much when the loading percentage of platinum metal on the surface of the catalyst increased from 0.25 wt.% to 0.5 wt.%, but the large increase of the resulting isomers appeared when the loaded metal was increased to 0.75 wt.% at different temperatures, while increasing the percentage of the loaded metal from 0.75 wt.% to 1 wt.% gave opposite results, as it led to a decrease in the resulting isomers. Metal loading on the catalyst surface is a

very accurate procedure because it greatly affects the generation of metallic sites on the surface of the catalyst as well as the distribution of these sites throughout its structural framework. The small number of metal functionalities can lead to a decrease in the efficiency of hydrogenation and dehydrogenation reactions, which play the main role in the production of isomers and catalytic selectivity. Increasing the percentage of metal loaded on the catalyst surface can close the opening pores and lead to a decrease in the initial hydrocracking reactions of the feedstock hydrocarbons, as it prevents the reactants from reaching many acidic sites, and as a result, the catalytic activity decreases in general [38,39]. Furthermore, it can be distinguished that 350 °C is the best reaction temperature at which the percentage of isomers production is achieved, taking into consideration that 350 °C is the critical boundary between hydroisomerisation and hydrocracking reactions. The reaction temperature is considered a major challenge in such catalytic reactions; unsurprisingly, the use of a higher temperature (i.e., 400 °C) leads to an increase in the hydrocracking reactions and the production of light gases along with an increase in the amount of coke accumulated at the expense of the hydroisomerisation reactions and the production of isomers [40,41]. On the other hand, a lower temperature (i.e., 300 °C) may not serve the purpose required for catalytic reactions to take place at a level sufficient to break down hydrocarbons or produce isomers over a specified reaction time. Therefore, a decrease in conversion is observed in most cases when the reaction temperature is reduced. Consequently, the reaction temperature must be controlled with great accuracy to obtain the highest possible product value [42]. Accordingly, it can be concluded that 0.75 wt.% of metal loaded onto the catalyst surface and conducting the reactions at a temperature of 350 °C gives the best criterion that can be used to obtain the greatest hydroisomerisation of the *n*-heptane components for the purpose of raising the octane number.

2.2. ANN Model Training

2.2.1. Training of Artificial Neural Networks (ANNs)

In fact, finding a suitable network with a minimal error in the training data is important and is achieved through careful selection of the number of neurons in the hidden layer. Different topologies having one or two hidden layer(s) of equal number of neurons were tested iteratively en route for obtaining the optimal ANN topology. The first layer is an input layer and consists of four neurons (i.e., reaction temperature, wt.% Pt-metal loaded, H_2/n-C_7 feed ratio, and weight-hourly space velocity (WHSV)). The second and third layers are hidden layers containing a variable number of neurons (1–30). The fourth layer is the output layer and contains twelve neurons (i.e., the mole fraction of products). ANN training is basically an optimisation process by which the weights of the neural network are altered for the purpose of minimising the error function. The most common error function used to quantify the performance of a neural network topology is the mean absolute error (MAE). In this work, a single hidden layer containing a single neuron was started, and this was followed by training and testing of the neural network. In order to improve the overall results of training and testing, the number of neurons was increased and this process was repeated each time. Several net configurations with one layer and two hidden layers were trained using input–output patterns. MAE values were estimated for each neural network topology. By comparing the values of MAE obtained of one and two hidden layers, as displayed in Figure 4a,b, respectively, it was found that a lower level of MAE was obtained by using two hidden layers having equal number of neurons compared to using one hidden layer, especially for 12 and 24 neurons. The optimum number of neurons in the hidden layer was also found to be 24 in this case. The lowest level of MAE (i.e., 0.5162) was achieved when two hidden layers with 24 neurons each were used; therefore, the 4–24–24–12 topology was chosen as the optimal ANN topology for the characterisation of hydroisomerisation and hydrocracking of *n*-heptane. A lower level of error was identified when using a number of neurons equal to or twice the number of dependent output variables. In addition, higher levels of error were achieved when 1–5 neurons were used for

both one and two hidden layers. Thereby, the best model developed in this study consists of four layers, as demonstrated in Figure 5.

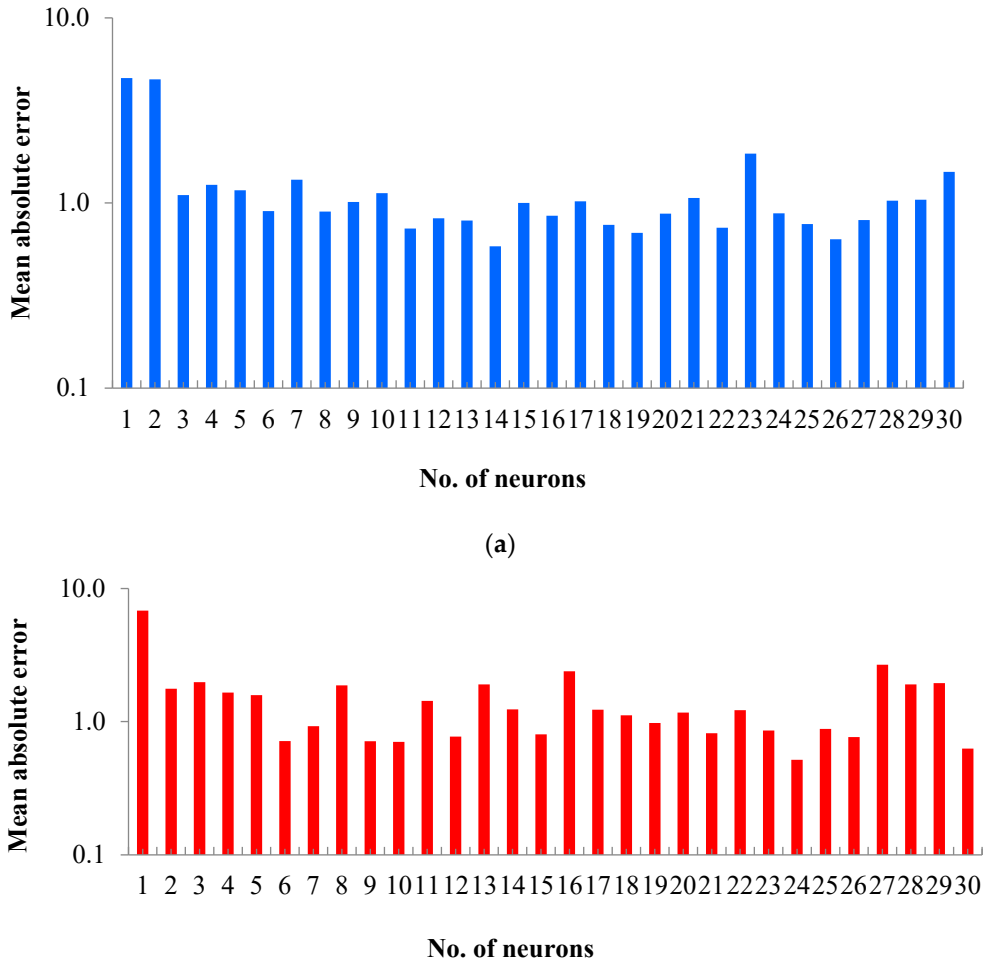

Figure 4. Mean absolute error achieved for different numbers of hidden layers and neurons: (**a**) one hidden layer and (**b**) two hidden layers of equal neurons.

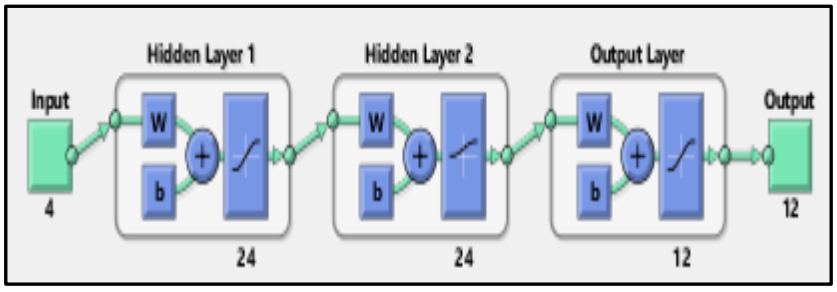

Figure 5. Optimum selected topology for ANN network.

The number of epochs indicates the number of iterations completed until the optimal value of the target function (i.e., the minimum value of the sum squared error, SSE) is finally reached. Obviously, the SSE value decreases as the number of iterations (epochs) increases. A value of 0.79858 was found as the lower limit for SSE when the epoch number reached 582, while a further increase in the epoch number had no significant effect on the SSE value. Accordingly, the maximum number of epochs was set at 582 during ANN

modelling. Figure 6 illustrates the error versus epochs. The parameters of the ANN model are summarised in Table 2.

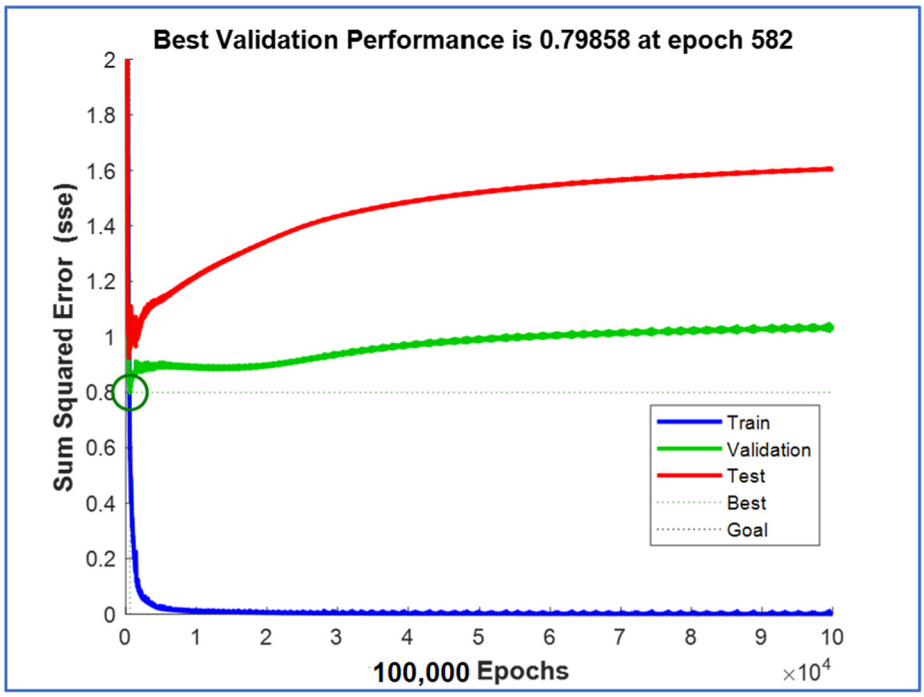

Figure 6. SSE predictions regarding the number of epochs.

Table 2. Parameters of artificial neural network model.

Input layer	Input data (4 variables)
Output layer	Composition of the products (12 variables)
Number of hidden layers	2
Number of neurons for each hidden layer	24
Performance function	Mean absolute error (MAE)
Activation function	Sigmoid
Type of activation sigmoid	Tan-sigmoid transfer function was used in first hidden layer Log-sigmoid transfer function was used in second hidden layer
Algorithm used for training	Levenberg–Marquardt
Learning rate	0.0001
Max number of iterations	1000
Gradient	0.00001

In addition, the strength of ANN model development is illustrated as parity plots and shown in Figure 7 for training, validation, and testing, in which the correlation coefficient (R^2) was found to be 0.9918, 0.9492, and 0.9426 for training, validation, and testing, respectively, and an average of 0.9767 for all data. According to the acceptable obtained level of correlation coefficient (R^2), which lies within the range of 0.95–1, it can be concluded that the ANN model accurately simulates hydrocracking and hydroisomerisation of *n*-heptane over a Pt-supported catalyst in the temperature range of 300–400 °C.

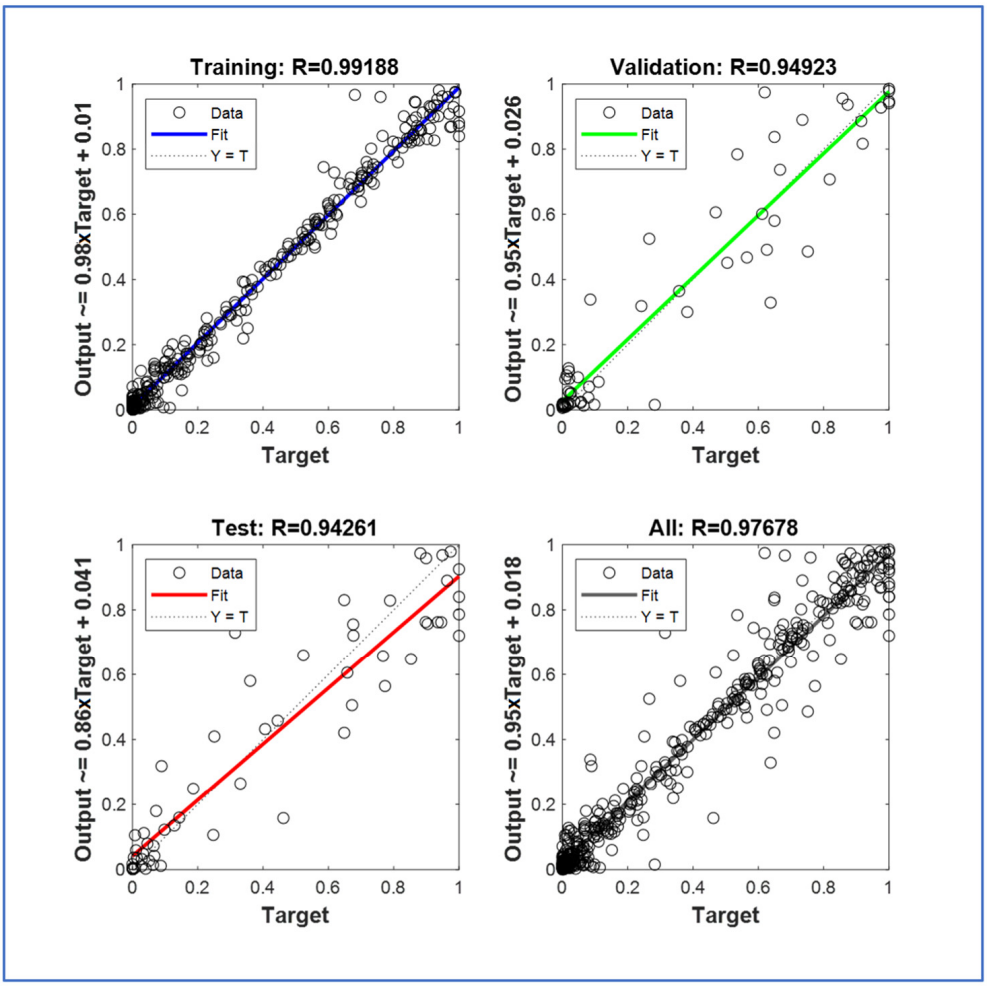

Figure 7. Predicted results versus experimental data.

2.2.2. Comparison of ANN Predictions

The predicted mole fractions calculated by the trained ANN were plotted against the experimental values, as shown in Figure 8. The observed correlation coefficient (R^2) for all components was greater than 0.926 except for *i*-C_5H_{12}, which had a correlation coefficient of the order of 0.767. It is noted that the applicability is high between the experimental and expected results, as the value of the correlation coefficient is always close to one. On the contrary, whenever the values are far from one, the mathematical model fails to represent the experimental results. For *i*-C_5H_{12}, the lower correlation coefficient can be attributed to the ANN optimisation algorithm using mean absolute error as an objective function during optimisation; therefore, the focus will be on components having higher mole fractions, contrary to the components having lower mole fractions such as *i*-C_5H_{12}, which has a maximum mole fraction of 0.8%. As mentioned earlier, the average correlation coefficient for all experiments and all components was found to be 0.9767, which is strongly accepted. On the strength of these findings, neural network modelling appears to be a better approach for modelling the behaviour of n-heptane hydroisomerisation and hydrocracking reactions on the surface of a bifunctional zeolite catalyst. MATLAB® Version 2020a was utilised to complete all required computations and predictions.

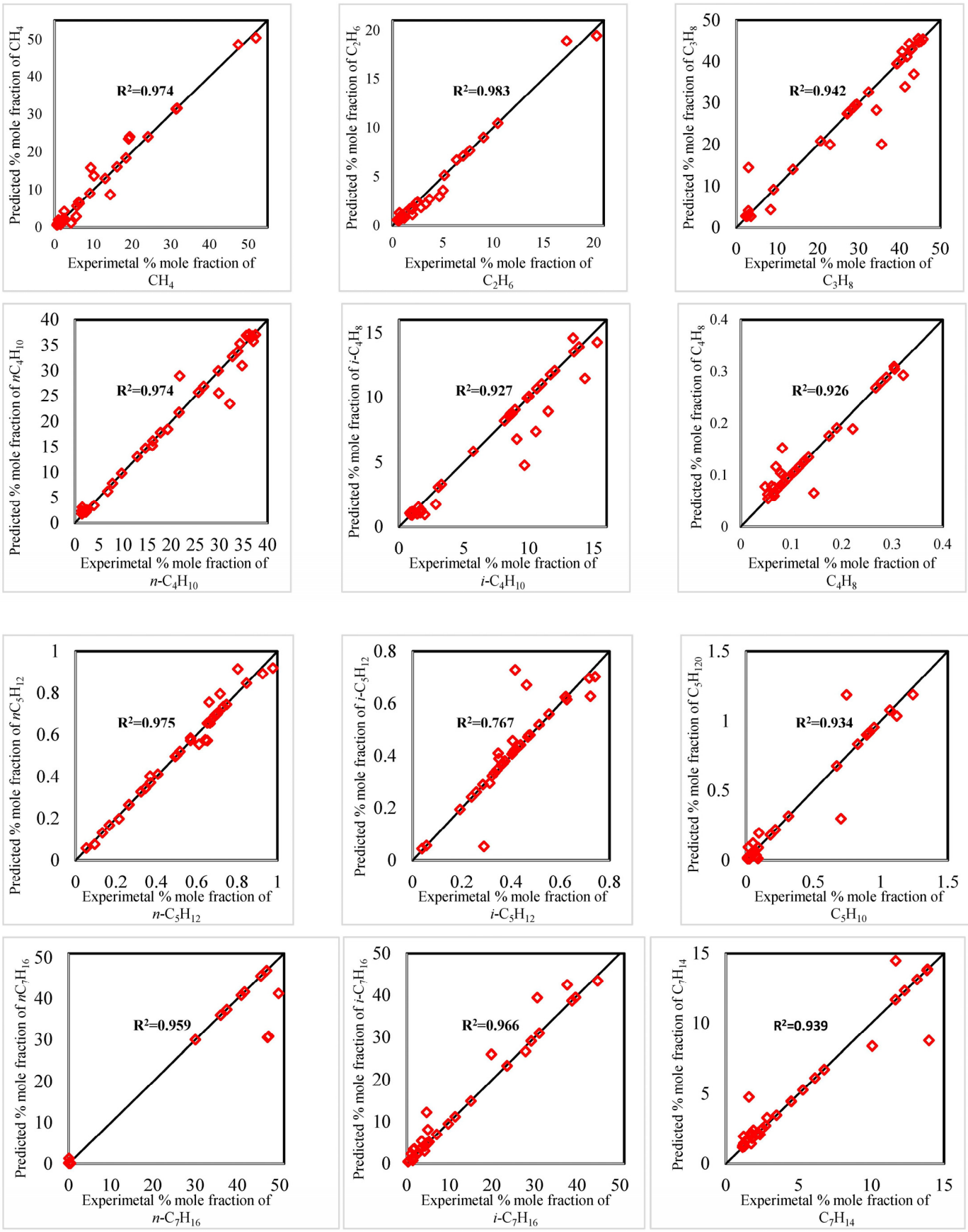

Figure 8. Comparison between the real and predicted mole fraction of product components.

2.2.3. Optimisation of Research Octane Number

The maximisation of the objective function (i.e., raising the *RON* value) via modelling and optimising the *n*-heptane hydrocracking and hydroisomerisation processes was achieved by using the hybrid artificial neural network–genetic algorithm (ANN–GA) approach. The details of the multiple steps of the hybrid ANN–GA approach taken in this study are easily illustrated by the pathways demonstrated in the flowchart in Figure 9. As a general rule, this flowchart can be divided into two main parts. The first part involves the development of a black box model based on the ANN methodological approach, so the inputs of the neural network are process parameters being optimised and the outputs of the neural network are also process parameters. In the second part, the optimal output was attained using GA, which was utilised to study the optimisation of the input variables of the ANN model. In other words, after the ANN model for the process was generated in the first part, GA was used in the second part for the purpose of optimising the four-dimensional space of the decision variables.

The optimisation results are summarised in Figure 10. In this figure, the objective function value (i.e., maximum *RON*) as well as the operating conditions with respect to the iteration number are plotted. The operating conditions (i.e., wt.% Pt-metal loaded, reaction temperature, H_2/*n*-heptane feed ratio, and WHSV) were changed iteratively within the specified range shown previously in Table 1. In fact, a maximum *RON* of 106.84 was achieved under optimal operating conditions: 0.85 wt.% Pt-metal loaded, 359.36 °C reaction temperature, 6.562 H_2/*n*-heptane feed ratio and 3.409 h^{-1} WHSV. Finally, it can be concluded that the results of this study have reached the optimal conditions to raise the RON value of the products in the hydroisomerisation and hydrocracking of *n*-heptane reactions, under the determinants of the main reaction parameters, which are both the percentage of platinum metal loaded on the surface of the catalyst and the reaction temperature, and these results are almost consistent with those of studies conducted by other researchers [43,44]. The higher reaction temperature was supposed to accelerate the rate of hydrocracking reactions at a temperature above 350 °C, as previously revealed in the experimental results discussion section, which consequently leads to a decrease in the *RON* of the products. Conversely, as the reaction temperature increases by about 10 °C, it is noted that the *RON* of the products continues to increase, possibly owing to the hydroisomerisation of hydrocarbon chains resulting from the hydrocracking reaction, which have five carbon atoms [45]. After the reaction temperature reaches 359.36 °C according to the results of the empirical model, it is seen that the production of isomers decreases; thus, the *RON* of the products decreases due to the increase in the rate of the hydrocracking reaction. In fact, raising the reaction temperature leads to a significant increase in the catalytic activity of the hydrocarbon cracking process, and this leads to an increase in the reaction conversion in general along with a decrease in selectivity towards the production of isomers [46].

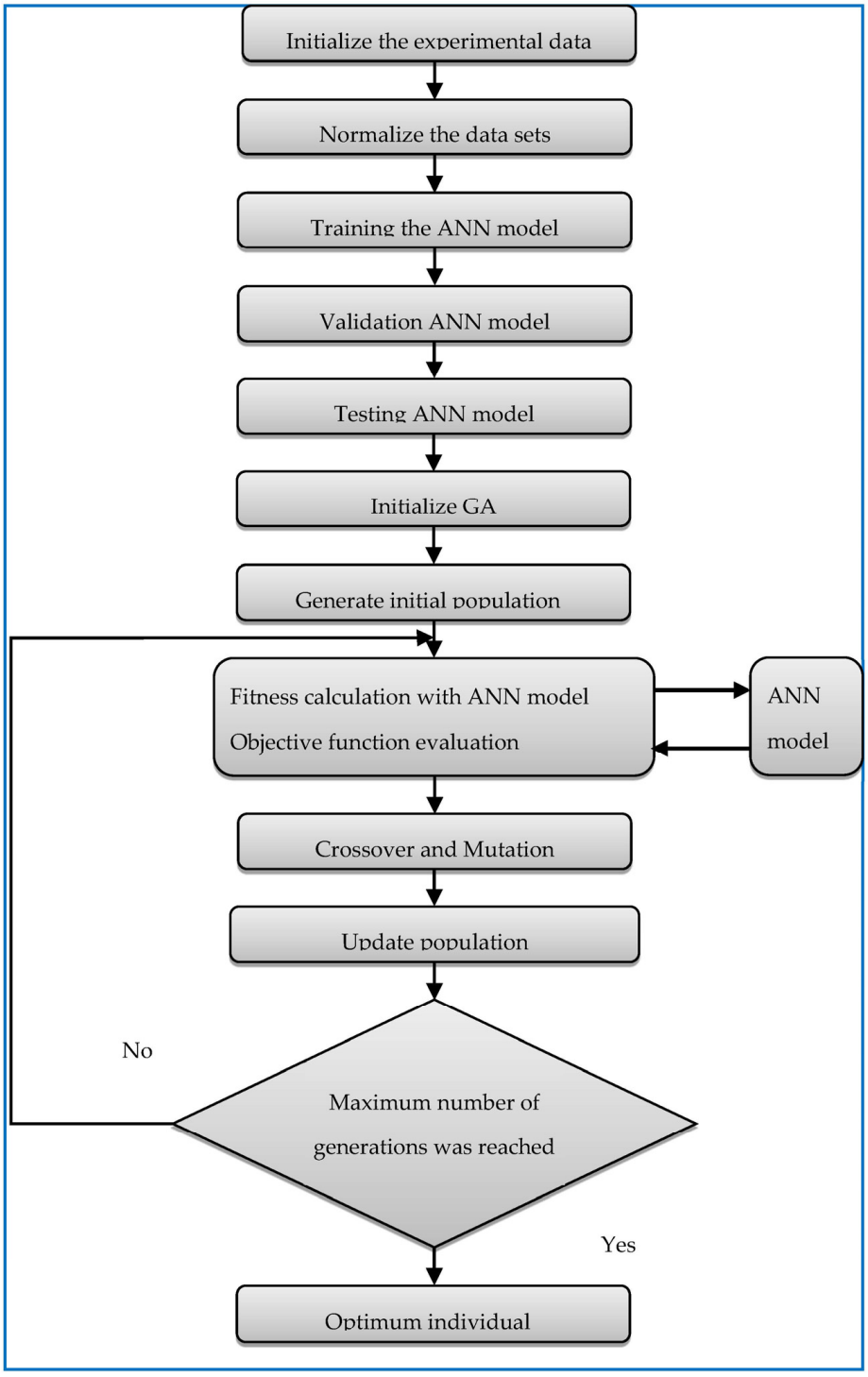

Figure 9. ANN–GA simulation–optimisation procedure flowchart.

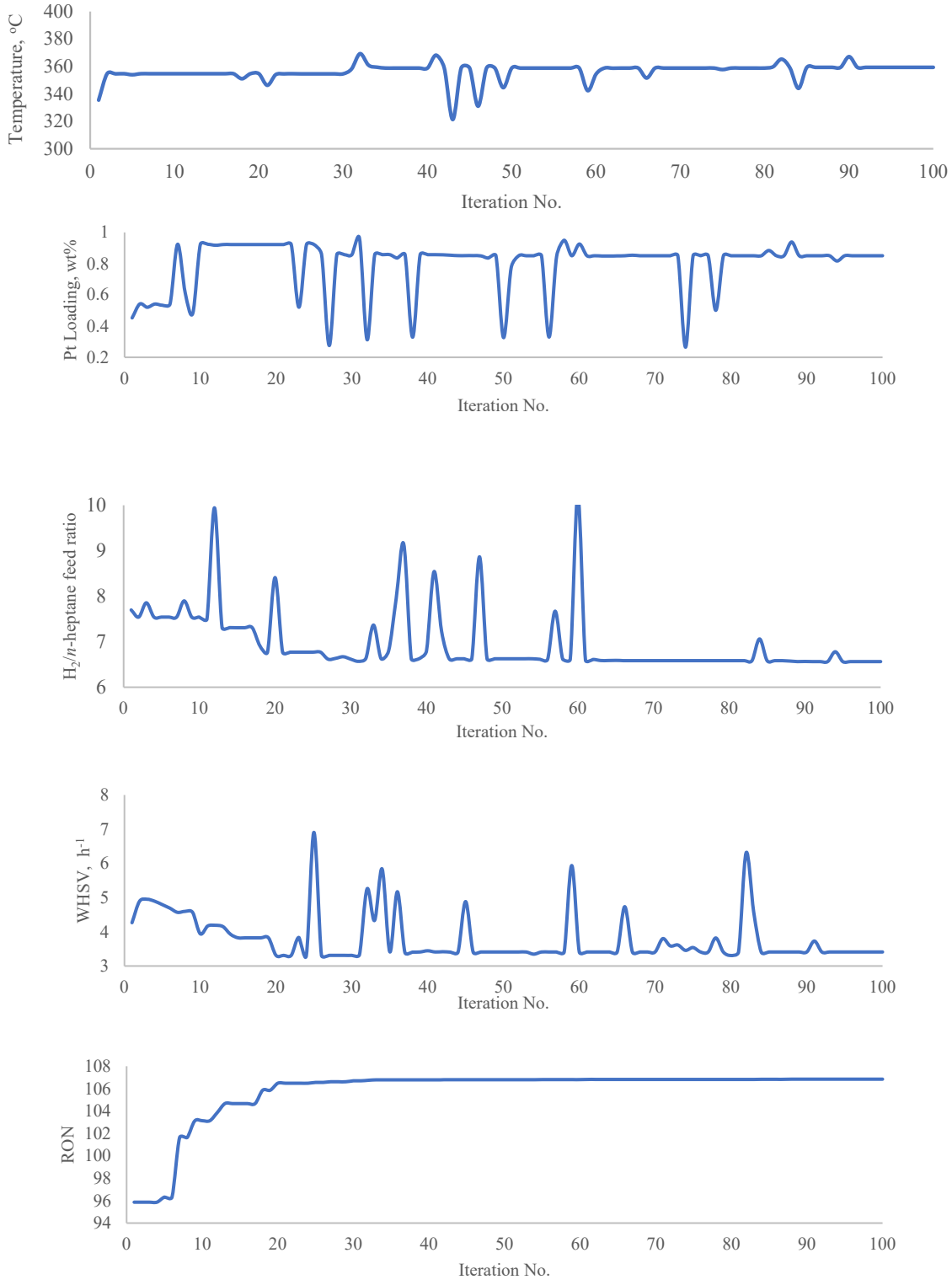

Figure 10. Optimisation of *RON* with the iteration number.

3. Experimental Work

In the heterogeneous process, hydroisomerisation and hydrocracking experiments were carried out for 99 wt.% liquid *n*-heptane with chemical formula [CH_3 $(CH_2)_5$ CH_3] from Sigma-Aldrich and having a boiling point in the range of 97–98 °C. Heptane has a zero point on the octane rating scale and was therefore chosen as a light *n*-alkane feedstock. The decationised catalysts provided by Alfa Aesar (45,867 Zeolite Y, ammonium) and (45,879 Zeolite ZSM-5, ammonium) with a SiO_2:Al_2O_3 mole ratio of 5.2:1 and 23:1 along

with a BET surface area of 750 and 425 m^2/g_{cat}, respectively, were used as a common standard catalyst for catalytic reactions. Then, 99.9% H_2PtCl_6 Hexa-ChloroPlatinic (IV) acid from Sigma-Aldrich with a molecular weight of 409.81 g/mol was used as a source of Pt-metal and loaded into the HY-ZSM-5 zeolite structures by common incipient wetness impregnation method [47] to obtain different percentages of 0.25, 0.5, 0.75, and 1 wt.% Pt-metal loaded according to the results of inductively coupled plasma analysis. A mixture of 75 wt.% HY and 25 wt.% HZSM-5 powdered catalysts loaded with Pt-metal was shaped into pellets of size about 150–450 µm. The bifunctional catalyst particles were then packed within a stable temperature zone inside a continuous-flow fixed-bed stainless-steel reactor, which was inserted in the middle of a vertical Carbolite® furnace. Prior to starting each experiment, streams of nitrogen gas followed by hydrogen gas coming from the cylinders in a steady flow using mass flow controllers (MFCs) were initially passed through purifiers to finally reach the catalyst bed separately for the purpose of activating the catalyst in situ inside the reactor. Then, 40 mL/min for 3 h of nitrogen gas was used for the calcination step to decompose NH_3 ions from the catalyst framework at 450 °C, after which a constant gas flow of 30 mL/min for 2 h of hydrogen gas was employed for metal reduction on the surface of de-ammoniated catalyst lattice at 350 °C. The hydrogen then passed as a carrier gas saturated with *n*-C_7H_{16} molecules through the pipes of the system, which were held at 120 °C using an electric heater and were also covered with an insulating layer of aluminium foil to avoid *n*-heptane vapor condensation; the reaction began when the feed contacted the granular catalyst bed, as shown in Figure 11. In a gas phase and under an atmospheric pressure, hydroisomerisation and/or hydrocracking reactions were performed over each mixture of HY-HZSM-5 catalyst loaded with a certain percentage of Pt-metal, 0.25 to 1 wt.%, at three different temperatures (e.g., 300, 350, and 400 °C). In addition, under each temperature, three total flow rates of 22.5, 38, and 57.5 mL/min (i.e., H_2:*n*-C_7 feed ratios were 6.5, 8.5, and 10.5, respectively) were used to obtain three different weight-hourly space velocity (e.g., WHSV = 2.98, 5.03, and 7.61 h^{-1}). Accordingly, a total of thirty-six experiments were conducted with twelve experiments at each temperature, as previously listed in Table 1, and the reaction products were analysed using gas chromatography. The molar percentage of isomers produced in each experiment was calculated using Equation (1) [48]:

$$\text{Selectivty} = \frac{(\text{Total moles of isomers})}{\text{Initial moles of nC}_7 - \text{Unreacted moles of nC}_7} * 100 \quad (1)$$

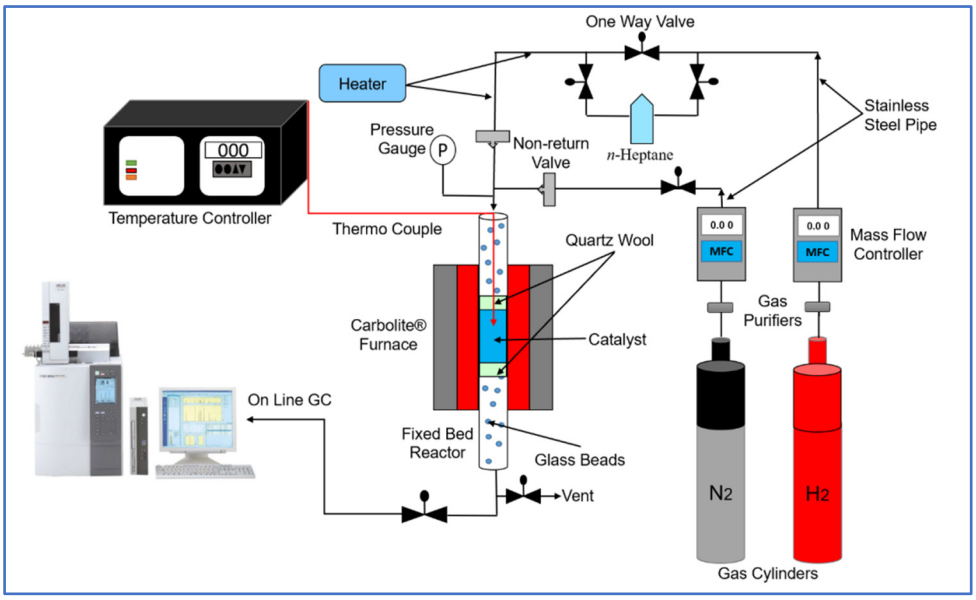

Figure 11. Experimental hydroisomerisation/hydrocracking laboratory rig.

4. Theoretical Work

4.1. Artificial Neural Network Modelling

ANN, which mimics the processes of the human brain, is basically a series of mathematical algorithms that are used in this study to estimate the relationships between datasets. ANN models are able to establish empirical relationships between dependent and independent variables based on a set of experimental data. The multilayer feedforward neural network (MFFNN) is currently the most popular topology in developing neural network models [49,50]. The ANN contains several layers, which are an input layer, a hidden layer(s), and an output layer. There may be a different number of neurons within each layer, and those neurons are connected to a weight that measures their strength.

The output of the *j*th and *k*th hidden nodes are given by Equations (2) and (3), respectively [51]:

$$\text{net}_j = \sum_{i=1}^{I} W_{i,j} x_i \tag{2}$$

$$\text{output}_j = f(\text{net}_j)$$

$$\text{net}_k = \sum_{n=1}^{N} W_{n,k} x_n \tag{3}$$

$$\text{output}_k = f(\text{net}_k)$$

In addition, transfer functions (i.e., sigmoid) arise between ANN layers, and their function is to link inputs and outputs. The three sigmoids commonly used in ANN models are linear (i.e., purelin), hyperbolic tangent sigmoid (i.e., tansig), and log-sigmoid (i.e., logsig) [52,53]. The tan-sigmoid and log-sigmoid transfer functions are given by Equations (4) and (5), respectively:

$$f(x) = \frac{2}{\left(1 + e^{-2x}\right)} - 1 = tansig(x) \tag{4}$$

$$f(x) = \frac{1}{\left(1 + e^{-x}\right)} = logsig(x) \tag{5}$$

By summing the incoming weighted signals of the hidden nodes which pass through a specific network activation function (i.e., sigmoid function, f_o) the ANN outputs can be obtained, as given in Equation (6) [54]:

$$y_j = f_o\left(\sum_{i=1}^{n} W_{i,j} x_i + b_j\right) \tag{6}$$

where x_i is the input variable, y_j is the output variables, b_j is a bias, $W_{i,j}$ is the weight from *i*th neuron in the *j*th layer, and f_o is the activation function of the *j*th neuron, which could be tansig or logsig sigmoid.

Designing an Artificial Neural Network

In general, there are three steps that can be followed in developing a neural network model. The first step involves generating the private data for training and the second step involves training the neural network using the selected data generated. It is worth noting that during this step, an objective function is employed to reduce the errors within the predicted and target values due to the fact that the network can be exposed to a certain number of patterns. The third step (e.g., testing) is the stage in which the accuracy of the predicted pattern is adjudged by the exposure of the trained network to an unfamiliar dataset.

The set of data points based on 36 laboratory experiments can be considered fairly suitable for modelling the neural network, and the success of the modelling is evident

from the empirical model being developed in the current study and can be very useful in optimising the experimental work. It can also be combined with other techniques such as statistical analysis (see Section 4.2), so that successful models can be built using a relatively small number of datasets [55–60]. Evidence for this is established by comparing the results of the optimal reaction conditions that will be obtained through the developed empirical model with the results obtained under original experimental reaction conditions, which should prove a high agreement between theoretical and experimental results. A total of 180 datasets were chosen for training and testing the neural network using the pregenerated multiple datasets (in a more precise sense, the 180 datasets were divided into 144 datasets for training and testing neural networks and the remaining 36 datasets were used for validation). In fact, 36 datasets represent the original experimental results. The 144 datasets were generated from experimental results using the response surface methodology (*RSM*) method, which is a set of mathematical and statistical methods aimed at analysing problems through an empirical model. The technique used in the current study is consistent with the techniques of other studies in the published literature [61–63].

The multilayer feedforward ANN model was used to estimate the performance of the *n*-heptane reactions and the selectivity of the products. In Figure 12, the artificial neurons can be described as representing a parallel, interconnected structure that includes (i) an input layer of neurons expressing independent variables, (ii) a number of hidden layers, and (iii) an output layer expressing dependent variables. Here, it is clear that the number of input neurons is 4 and the number of output neurons is 12. The ANN model input contained four nodes represented by reaction temperature, wt.% Pt-metal loaded within the catalyst, H_2/n-C_7 feed ratio, and weight-hourly space velocity (WHSV), while the model output contained 12 nodes represented by the mole fractions produced (i.e., methane: CH_4, ethane: C_2H_6, propane: C_3H_8, butane: n-C_4H_{10}, isobutane: i-C_4H_{10}, butene: C_4H_8, pentane: n-C_5H_{12}, isopentane: i-C_5H_{12}, pentene: C_5H_{10}, heptane: n-C_7H_{16}, isoheptane: i-C_7H_{16}, and heptene: C_7H_{14}).

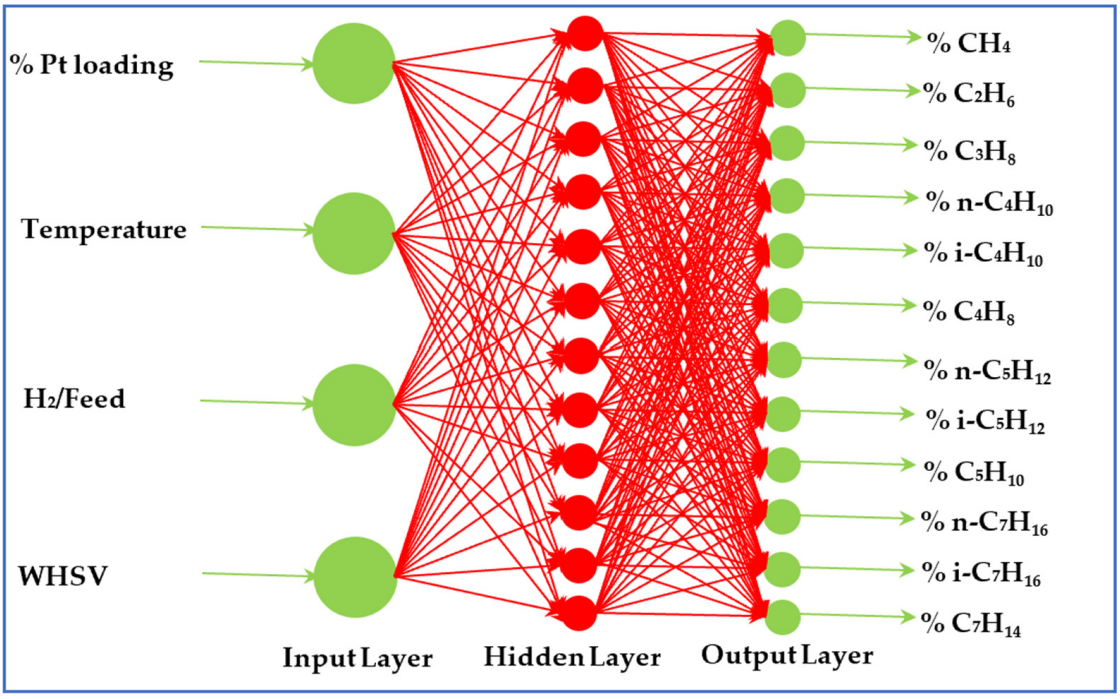

Figure 12. Artificial neural network structure.

According to the range of input and output datasets that is shown in Table 3, a significant difference between these variables can be recognized, where the mole fractions are within the range of 0–1, while the reaction temperature is within the range 300–400 °C. Normalisation is necessary when there are different ranges of the input and/or output

dataset. The ANN training model without normalisation will make optimisation (i.e., minimisation of objective function or error) focus on the variables with larger values. Using min–max normalisation is one of the most common methods of data normalisation, in which the range of datasets for different variables is converted from minimum–maximum (i.e., $x_{min}-x_{max}$) to 0–1. For each present feature, the maximum value of this feature is converted to (1), while the minimum value is converted to (0), and the remaining values are transformed into a decimal number between the (0) value and the (1) value. The input variables were normalised according to Equation (7) [64]:

$$x_i^{norm} = \frac{x_i - x_{min}}{x_{max} - x_{min}} \tag{7}$$

Table 3. Range of ANN model variables.

Maximum	Minimum	Variables
Temperature (°C)	300	400
Pt-metal loaded (wt.%)	0.25	1
H2/n-C7 feed ratio	6.5	10.5
WHSV (h−1)	2.98	7.61
Mole fraction (%)	0	1

In neural networks, training and testing are expressed by calibration and verification of mathematical models. Therefore, all variables prior to and subsequent to the actual application in the neural network are normalised and denormalised between the values of (1) and (0). By determining the minimum and maximum values for each variable during the entire data period, this process can be implemented, and the measured variables are calculated using Equation (8):

$$x_i = x_{min} + x_i^{norm}(x_{max} - x_{min}) \tag{8}$$

4.2. Statistical Analysis

Four different evaluating criteria were applied to compare the experimental and predicted results, in which correlation coefficient of determination (R^2), mean absolute error (*MAE*), mean relative error (*MRE*), and mean square error (*MSE*) were calculated using Equations (9)–(12) [65]:

$$R^2 = 1 - \frac{\sum_{i=1}^{N}\left(y_{exp,i} - y_{pred,i}\right)^2}{\sum_{i=1}^{N}\left(y_{exp,i} - \overline{y}_{exp}\right)^2} \tag{9}$$

$$MAE = \frac{1}{N \times M}\sum_{j=1}^{M}\sum_{i=1}^{N}\left|y_{i,j}^{exp} - y_{i,j}^{pred}\right| \tag{10}$$

$$MRE = \frac{1}{N \times M}\sum_{j=1}^{M}\sum_{i=1}^{N}\left(\frac{y_{i,j}^{exp} - y_{i,j}^{pred}}{y_{i,j}^{exp}}\right) \tag{11}$$

$$MSE = \frac{1}{N \times M}\sum_{j=1}^{M}\sum_{i=1}^{N}\left(y_{i,j}^{exp} - y_{i,j}^{pred}\right) \tag{12}$$

where $y_{i,j}$ is the mole fraction of *i*th component in *j*th experiments, *M* represents the number of experiments, *N* represents the number of components, and *exp.* and *pred.* are superscripts denoting to experimental and predicted results.

4.3. Optimisation Method

The genetic algorithm (GA) optimisation method was also used to select the optimum operating conditions. The ANN model was employed to evaluate the model output for each selected chromosome (i.e., values of operating conditions). The GA optimisation method was utilized to predict the operating conditions which corresponded to prediction maximum octane number (i.e., research octane rating, *RON*). The *RON* of a mixture explicitly expresses the sum of the contributions of each component within that mixture and can be calculated according to Equation (13) [4]:

$$RON = \sum_{i=1}^{nc} \alpha_i \times RON_i \quad (13)$$

where *RON* is a measure of the octane number of all hydrocarbons produced, whereas RON_i is the octane number of only the pure component of each *i*-molecule within that product, and α_i is an expression of the volumetric fractions of the reaction products.

5. Conclusions

In the present study, *n*-heptane hydroisomerisation and hydrocracking were modelled. The operating conditions were optimised using both artificial neural network (ANN) and genetic algorithm (GA) in tandem to enhance the research octane number (*RON*) value of the reaction products. For the purpose of constructing an optimal ANN model having a 4–24–24–12 topology, the parameters of the ANN model were optimised. In order to investigate the regression model developed in this study, the predicted values and the actual values were compared in combination with a small percentage of error. The results of the comparison confirmed that it is possible to rely on the developed model to predict the conversions of the reactant and, thus, the selectivity of the reaction products within the range of operating conditions used in this study. In conclusion, the results show that ANNs are a suitable tool for evaluating even highly complex and nonlinear reaction systems. Moreover, with a correlation coefficient (R^2) of 0.9767, the developed ANN model was able to provide an accurate prediction for all the used experimental data. Finally, applications of the genetic algorithm were utilised to optimize the reaction conditions during the process towards increasing the octane number of the products. The maximum *RON* value of 106.84 was achieved under the optimal operating conditions of 0.85 wt.% Pt-metal loaded, 359.36 °C, 6.562 H_2/*n*-heptane feed ratio, and 3.409 h^{-1} WHSV. The results of the optimal conditions for the reactions obtained through the developed empirical model are in agreement with the experimental results. Through conducting 36 experiments of *n*-heptane hydroisomerisation/hydrocracking reactions on the surface of the bifunctional HY-HZSM-5 catalyst, the highest percentage of the resulting isomers was found with about 78.7 mol% on the surface of the zeolite catalyst loaded with 0.75 wt.% Pt-metal at 350 °C using the feed ratio of 6.5 H_2/*n*-C_7 and WHSV of 2.98 h^{-1}.

Author Contributions: Conceptualization, B.Y.A.-Z. and A.A.-S.; methodology, A.K.S.; software, Z.M.S.; validation, A.A.A., H.S.M. and Z.M.S.; formal analysis, B.Y.A.-Z. and A.K.S.; investigation, A.A.-S.; resources, B.Y.A.-Z. and Z.M.S.; data curation, B.Y.A.-Z. and A.A.-S.; writing—original draft preparation, B.Y.A.-Z., A.A.-S. and Z.M.S.; writing—review and editing, A.A.A.; visualization, J.M.; supervision, A.A.A. and J.M.; project administration, H.S.M.; funding acquisition. All authors have read and agreed to the published version of the manuscript.

Funding: This research received no external funding.

Data Availability Statement: All relevant data are included in the paper.

Acknowledgments: The authors are grateful to the Chemical Engineering Department, University of Technology, Baghdad, Iraq, and Al-Mustaqbal University College, Hilla, Babylon, Iraq, for providing support and facilities to accomplish this work.

Conflicts of Interest: We certify that they have no affiliations with or involvement in any organization or entity with any financial interest or nonfinancial interest in the subject matter or materials discussed in this manuscript.

Abbreviations

ANN–GA	Hybrid artificial neural network–genetic algorithm
ANNs	Artificial neural networks
b_j	User bias
exp.	Superscripts letters indicate experimental results
FF–ANN	Feedforward artificial neural network
f_o	Sigmoid function, which is the activation function of the *j*th neuron
GA	Genetic algorithm
*j*th and *k*th	Hidden nodes
M	Number of experiments
MAE	Mean absolute error
MFF–ANN	Multilayer feedforward artificial neural network
MRE	Mean relative error
MSE	Mean square error
N	Number of components
pred.	Superscripts letters indicate predicted results
R^2	Correlation coefficient
RSM	Response surface methodology.
RON	Research octane number of all hydrocarbons produced
RON_i	Octane number of only the pure component of each *i*-molecule within that product
SSE	Sum of square error
W/F	Weight of the catalyst divided by the molar flow rate of *n*-C_7 in the feed
WHSV	Weight-hourly space velocity
$W_{i,j}$	Weight from *i*th neuron in the *j*th layer
x_i	Input variable
$y_{i,j}$	Mole fraction of *i*th component in *j*th experiments
y_j	Output variables
α_i	Volumetric fractions of the reaction products
Ø	Maximum free pore diameter

References

1. Al-Shafei, E.N.; Albahar, M.Z.; Aljishi, M.F.; Akah, A.; Aljishi, A.N.; Alasseel, A. Catalytic conversion of heavy naphtha to reformate over the phosphorus-ZSM-5 catalyst at a lower reforming temperature. *RSC Adv.* **2022**, *12*, 25465–25477. [CrossRef]
2. Fedyna, M.; Śliwa, M.; Jaroszewska, K.; Trawczyński, J. Effect of zeolite amount on the properties of Pt/(AlSBA-15 + Beta zeolite) micro-mesoporous catalysts for the hydroisomerization of n-heptane. *Fuel* **2020**, *280*, 118607. [CrossRef]
3. Gholami, Z.; Gholami, F.; Tišler, Z.; Vakili, M. A Review on the Production of Light Olefins Using Steam Cracking of Hydrocarbons. *Energies* **2021**, *14*, 8190. [CrossRef]
4. Shakor, Z.M.; Ramos, M.J.; AbdulRazak, A.A. A detailed reaction kinetic model of light naphtha isomerization on Pt/zeolite catalyst. *J. King Saud Univ. Eng. Sci.* **2022**, *34*, 303–308. [CrossRef]
5. Agarwal, U.; Rigutto, M.S.; Zuidema, E.; Jansen, A.; Poursaeidesfahani, A.; Sharma, S.; Dubbeldam, D.; Vlugt, T.J. Kinetics of zeolite-catalyzed heptane hydroisomerization and hydrocracking with CBMC-modeled adsorption terms: Zeolite Beta as a large pore base case. *J. Catal.* **2022**, *415*, 37–50. [CrossRef]
6. Jaroszewska, K.; Fedyna, M.; Trawczyński, J. Hydroisomerization of long-chain n-alkanes over Pt/AlSBA-15+zeolite bimodal catalysts. *Appl. Catal. B Environ.* **2019**, *255*, 117756. [CrossRef]
7. Melián-Cabrera, I. Catalytic Materials: Concepts to Understand the Pathway to Implementation. *Ind. Eng. Chem. Res.* **2021**, *60*, 18545–18559. [CrossRef]
8. Hamied, R.S.; Sukkar, K.A.; Majdi, H.S.; Shnain, Z.Y.; Graish, M.S.; Mahmood, L.H. Catalytic-Level Identification of Prepared Pt/HY, Pt-Zn/HY, and Pt-Rh/HY Nanocatalysts on the Reforming Reactions of N-Heptane. *Processes* **2023**, *11*, 270. [CrossRef]
9. Gomez, L.Q.; Shehab, A.K.; Al-Shathr, A.; Ingram, W.; Konstantinova, M. H_2-free Synthesis of Aromatic, Cyclic and Linear Oxygenates from CO_2. *ChemSusChem* **2020**, *13*, 647–658. [CrossRef]
10. Quintana-Gómez, L.; Connolly, M.; Shehab, A.K.; Al-Shathr, A.; McGregor, J. "Reverse combustion" of carbon dioxide in water: The influence of reaction conditions. *Front. Energy Res.* **2022**, *10*, 917943. [CrossRef]

11. Dai, X.; Cheng, Y.; Si, M.; Wei, Q.; Zhou, Y. Hydroisomerization of n-Hexadecane Over Nickel-Modified SAPO-11 Molecular Sieve-Supported NiWS Catalysts: Effects of Modification Methods. *Front. Chem.* **2022**, *10*, 857473. [CrossRef] [PubMed]
12. Mendes, P.S.; Lapisardi, G.; Bouchy, C.; Rivallan, M.; Silva, J.M.; Ribeiro, M.F. Hydrogenating activity of Pt/zeolite catalysts focusing acid support and metal dispersion influence. *Appl. Catal. A Gen.* **2015**, *504*, 17–28. [CrossRef]
13. Gao, S.-B.; Zhao, Z.; Lu, X.-F.; Chi, K.-B.; Duan, A.-J.; Liu, Y.-F.; Meng, X.-B.; Tan, M.-W.; Yu, H.-Y.; Shen, Y.-G.; et al. Hydrocracking diversity in n-dodecane isomerization on Pt/ZSM-22 and Pt/ZSM-23 catalysts and their catalytic performance for hydrodewaxing of lube base oil. *Pet. Sci.* **2020**, *17*, 1752–1763. [CrossRef]
14. Yilmaz, B.; Müller, U. Catalytic Applications of Zeolites in Chemical Industry. *Top. Catal.* **2009**, *52*, 888–895. [CrossRef]
15. Zhang, H.; bin Samsudin, I.; Jaenicke, S.; Chuah, G.-K. Zeolites in catalysis: Sustainable synthesis and its impact on properties and applications. *Catal. Sci. Technol.* **2022**, *12*, 6024–6039. [CrossRef]
16. Busca, G. *Heterogeneous Catalytic Materials*; Elsevier: Amsterdam, The Netherlands, 2014.
17. Ibarra, Á.; Hita, I.; Arandes, J.M.; Bilbao, J. A Hybrid FCC/HZSM-5 Catalyst for the Catalytic Cracking of a VGO/Bio-Oil Blend in FCC Conditions. *Catalysts* **2020**, *10*, 1157. [CrossRef]
18. Schmutzler, F.; Zschiesche, C.; Titus, J.; Poppitz, D.; Freiding, J.; Rakoczy, R.; Reitzmann, A.; Gläser, R. Hydroisomerization of Renewable and Fossil n-Alkanes over Bifunctional Dealuminated ZSM-5 Catalysts. *Chem. Ing. Tech.* **2021**, *93*, 981–989. [CrossRef]
19. Kazakov, M.O.; Smirnova, M.Y.; Dubinin, M.E.; Bogomolova, T.S.; Dik, P.P.; Golubev, I.S.; Revyakin, M.E.; Klimov, O.V.; Noskov, A.S. Combining USY and ZSM-23 in Pt/zeolite hydrocracking catalyst to produce diesel and lube base oil with improved cold flow properties. *Fuel* **2023**, *344*, 128085. [CrossRef]
20. Schweitzer, J.-M.; Rey, J.; Bignaud, C.; Bučko, T.; Raybaud, P.; Moscovici-Mirande, M.; Portejoie, F.; James, C.; Bouchy, C.; Chizallet, C. Multiscale Modeling as a Tool for the Prediction of Catalytic Performances: The Case of *n*-Heptane Hydroconversion in a Large-Pore Zeolite. *ACS Catal.* **2022**, *12*, 1068–1081. [CrossRef]
21. Song, W.; Mahalec, V.; Long, J.; Yang, M.-L.; Qian, F. Modeling the Hydrocracking Process with Deep Neural Networks. *Ind. Eng. Chem. Res.* **2020**, *59*, 3077–3090. [CrossRef]
22. Vandegehuchte, B.; Thybaut, J.; Martínez, A.; Arribas, M.; Marin, G. n-Hexadecane hydrocracking Single-Event MicroKinetics on Pt/H-beta. *Appl. Catal. A Gen.* **2012**, *441–442*, 10–20. [CrossRef]
23. Choudhury, I.R.; Hayasaka, K.; Thybaut, J.W.; Narasimhan, C.L.; Denayer, J.F.; Martens, J.A.; Marin, G.B. Pt/H-ZSM-22 hydroisomerization catalysts optimization guided by Single-Event MicroKinetic modeling. *J. Catal.* **2012**, *290*, 165–176. [CrossRef]
24. Martens, G.; Marin, G.; Martens, J.; Jacobs, P.; Baron, G. A Fundamental Kinetic Model for Hydrocracking of C8 to C12 Alkanes on Pt/US–Y Zeolites. *J. Catal.* **2000**, *195*, 253–267. [CrossRef]
25. Bricker, M.; Thakkar, V.; Petri, J. Hydrocracking in Petroleum Processing. In *Handbook of Petroleum Processing*; Treese, S.A., Pujadó, P.R., Jones, D.S.J., Eds.; Springer International Publishing: Cham, Switzerland, 2015; pp. 317–359.
26. Hamied, R.S.; Shakor, Z.M.; Sadeiq, A.H.; Razak, A.A.A.; Khadim, A.T. Kinetic Modeling of Light Naphtha Hydroisomerization in an Industrial Universal Oil Products Penex™ Unit. *Energy Eng.* **2023**, *120*, 1371–1386. [CrossRef]
27. Al-Shathr, A.; Shakor, Z.M.; Al-Zaidi, B.Y.; Majdi, H.S.; AbdulRazak, A.A.; Aal-Kaeb, S.; Shohib, A.A.; McGregor, J. Reaction Kinetics of Cinnamaldehyde Hydrogenation over Pt/SiO_2: Comparison between Bulk and Intraparticle Diffusion Models. *Int. J. Chem. Eng.* **2022**, *2022*, 8303874. [CrossRef]
28. Maghami, S.; Mehrabani-Zeinabad, A.; Sadeghi, M.; Sánchez-Laínez, J.; Zornoza, B.; Téllez, C.; Coronas, J. Mathematical modeling of temperature and pressure effects on permeability, diffusivity and solubility in polymeric and mixed matrix membranes. *Chem. Eng. Sci.* **2019**, *205*, 58–73. [CrossRef]
29. Al-Shathr, A.; Shakor, Z.M.; Majdi, H.S.; AbdulRazak, A.A.; Albayati, T.M. Comparison between Artificial Neural Network and Rigorous Mathematical Model in Simulation of Industrial Heavy Naphtha Reforming Process. *Catalysts* **2021**, *11*, 1034. [CrossRef]
30. Shakor, Z.M.; Abdulrazak, A.A.; Sukkar, K. A Detailed Reaction Kinetic Model of Heavy Naphtha Reforming. *Arab. J. Sci. Eng.* **2020**, *45*, 7361–7370. [CrossRef]
31. Galvan, D.; Cremasco, H.; Mantovani, A.C.G.; Bona, E.; Killner, M.; Borsato, D. Kinetic study of the transesterification reaction by artificial neural networks and parametric particle swarm optimization. *Fuel* **2020**, *267*, 117221. [CrossRef]
32. Tai, X.Y.; Ocone, R.; Christie, S.D.; Xuan, J. Multi-objective optimisation with hybrid machine learning strategy for complex catalytic processes. *Energy AI* **2022**, *7*, 100134. [CrossRef]
33. Baş, D.; Dudak, F.C.; Boyacı, İ.H. Modeling and optimization III: Reaction rate estimation using artificial neural network (ANN) without a kinetic model. *J. Food Eng.* **2007**, *79*, 622–628. [CrossRef]
34. Gusmão, G.S.; Retnanto, A.P.; da Cunha, S.C.; Medford, A.J. Kinetics-informed neural networks. *Catal. Today* **2023**, *417*, 113701. [CrossRef]
35. Gomes, L.C.; Rosas, D.D.O.; Chistone, R.C.; Zotin, F.M.Z.; de Araujo, L.R.R.; Zotin, J.L. Hydroisomerization of n-hexadecane using Pt/alumina-Beta zeolite catalysts for producing renewable diesel with low pour point. *Fuel* **2017**, *209*, 521–528. [CrossRef]
36. Jiménez, C.; Romero, F.J.; Roldán, R.; Marinas, J.M.; Gómez, J.P. Hydroisomerization of a hydrocarbon feed containing n-hexane, n-heptane and cyclohexane on zeolite-supported platinum catalysts. *Appl. Catal. A Gen.* **2003**, *249*, 175–185. [CrossRef]
37. Mäki-Arvela, P.; Khel, T.A.K.; Azkaar, M.; Engblom, S.; Murzin, D.Y. Catalytic Hydroisomerization of Long-Chain Hydrocarbons for the Production of Fuels. *Catalysts* **2018**, *8*, 534. [CrossRef]
38. Žula, M.; Grilc, M.; Likozar, B. Hydrocracking, hydrogenation and hydro-deoxygenation of fatty acids, esters and glycerides: Mechanisms, kinetics and transport phenomena. *Chem. Eng. J.* **2022**, *444*, 136564. [CrossRef]

39. Wang, W.; Liu, C.-J.; Wu, W. Bifunctional catalysts for the hydroisomerization of *n*-alkanes: The effects of metal–acid balance and textural structure. *Catal. Sci. Technol.* **2019**, *9*, 4162–4187. [CrossRef]
40. Du, H.; Liu, D.; Li, M.; Wu, P.; Yang, Y. Effects of the Temperature and Initial Hydrogen Pressure on the Isomerization Reaction in Heavy Oil Slurry-Phase Hydrocracking. *Energy Fuels* **2015**, *29*, 626–633. [CrossRef]
41. Al-Shathr, A.; Al-Zaidi, B.Y.; Shehab, A.K.; Shakoor, Z.M.; Aal-Kaeb, S.; Gomez, L.Q.; Majdi, H.S.; Al-Shafei, E.N.; AbdulRazak, A.A.; McGregor, J. Experimental and kinetic studies of the advantages of coke accumulation over Beta and Mordenite catalysts according to the pore mouth catalysis hypothesis. *Catal. Commun.* **2023**, *181*, 106718. [CrossRef]
42. Al-Iessa, M.S.; Al-Zaidi, B.Y.; Almukhtar, R.S.; Shakor, Z.M.; Hamawand, I. Optimization of Polypropylene Waste Recycling Products as Alternative Fuels through Non-Catalytic Thermal and Catalytic Hydrocracking Using Fresh and Spent Pt/Al_2O_3 and $NiMo/Al_2O_3$ Catalysts. *Energies* **2023**, *16*, 4871. [CrossRef]
43. Ali, N.S.; Alismaeel, Z.T.; Majdi, H.S.; Salih, H.G.; Abdulrahman, M.A.; Saady, N.M.C.; Albayati, T.M. Modification of SBA-15 mesoporous silica as an active heterogeneous catalyst for the hydroisomerization and hydrocracking of n-heptane. *Heliyon* **2022**, *8*, e09737. [CrossRef] [PubMed]
44. Calemma, V.; Peratello, S.; Perego, C. Modeling and Simulation of the Isomerization of n-Heptane over a Molybdenum Oxycarbide Catalyst for Elucidation of the Bifunctional Mechanism. Industrial & Engineering Chemistry Research. *Appl. Catal. A Gen.* **2023**, *62*, 9607–9618.
45. Calemma, V.; Peratello, S.; Perego, C. Hydroisomerization and hydrocracking of long chain n-alkanes on Pt/amorphous SiO2–Al2O3 catalyst. *Appl. Catal. A Gen.* **2000**, *190*, 207–218. [CrossRef]
46. Raseev, S. *Thermal and Catalytic Processes in Petroleum Refining*; CRC Press: Boca Raton, FL, USA, 2003.
47. Khalaf, Y.H.; Al-Zaidi, B.Y.S.; Shakour, Z.M. Experimental and Kinetic Study of the Effect of using Zr- and Pt-loaded Metals on Y-zeolite-based Catalyst to Improve the Products of n-heptane Hydroisomerization Reactions. *Orbital Electron. J. Chem.* **2022**, *14*, 153–167. [CrossRef]
48. Alemán-Vázquez, L.O.; Cano-Domínguez, J.L.; Torres-García, E.; Villagómez-Ibarra, J.R. Industrial application of catalytic systems for n-heptane isomerization. *Molecules* **2011**, *16*, 5916–5927. [CrossRef]
49. Malayeri, M.; Nasiri, F.; Haghighat, F.; Lee, C.-S. Optimization of photocatalytic oxidation reactor for air purifier design: Application of artificial neural network and genetic algorithm. *Chem. Eng. J.* **2023**, *462*, 142186. [CrossRef]
50. Kirilova, E.G. Artificial Neural Networks: Applications in Chemical Engineering. In *Modeling and Simulation in Chemical Engineering: Project Reports on Process Simulation*; Boyadjiev, C., Ed.; Springer International Publishing: Cham, Switzerland, 2022; pp. 127–146.
51. Elçiçek, H.; Akdoğan, E.; Karagöz, S. The Use of Artificial Neural Network for Prediction of Dissolution Kinetics. *Sci. World J.* **2014**, *2014*, 194874. [CrossRef]
52. Vogl, T.P.; Mangis, J.K.; Rigler, A.K.; Zink, W.T.; Alkon, D.L. Accelerating the convergence of the back-propagation method. *Biol. Cybern.* **1988**, *59*, 257–263. [CrossRef]
53. Govindan, B.; Jakka, S.C.B.; Radhakrishnan, T.K.; Tiwari, A.K.; Sudhakar, T.M.; Shanmugavelu, P.; Kalburgi, A.K.; Sanyal, A.; Sarkar, S. Investigation on Kinetic Parameters of Combustion and Oxy-Combustion of Calcined Pet Coke Employing Thermogravimetric Analysis Coupled to Artificial Neural Network Modeling. *Energy Fuels* **2018**, *32*, 3995–4007. [CrossRef]
54. Demir, B.; Eski, I.; Gürbüz, F.; Kuş, Z.A.; Sesli, Y.; Ercişli, S. Prediction of Walnut Mass Based on Physical Attributes by Artificial Neural Network (ANN). *Erwerbs-Obstbau* **2020**, *62*, 47–56. [CrossRef]
55. Abdul Rahman, M.B.; Chaibakhsh, N.; Basri, M.; Salleh, A.B.; Rahman, R.N.Z.R.A. Application of Artificial Neural Network for Yield Prediction of Lipase-Catalyzed Synthesis of Dioctyl Adipate. *Appl. Biochem. Biotechnol.* **2009**, *158*, 722–735. [CrossRef] [PubMed]
56. Betiku, E.; Ajala, S.O. Modeling and optimization of Thevetia peruviana (yellow oleander) oil biodiesel synthesis via Musa paradisiacal (plantain) peels as heterogeneous base catalyst: A case of artificial neural network vs. response surface methodology. *Ind. Crop. Prod.* **2014**, *53*, 314–322. [CrossRef]
57. Hafizi, A.; Ahmadpour, A.; Koolivand-Salooki, M.; Heravi, M.M.; Bamoharram, F.F. Comparison of RSM and ANN for the investigation of linear alkylbenzene synthesis over H14[NaP5W30O110]/SiO_2 catalyst. *J. Ind. Eng. Chem.* **2013**, *19*, 1981–1989. [CrossRef]
58. Kasiri, M.B.; Aleboyeh, H. Modeling and Optimization of Heterogeneous Photo-Fenton Process with Response Surface Methodology and Artificial Neural Networks. *Environ. Sci. Technol.* **2008**, *42*, 7970–7975. [CrossRef] [PubMed]
59. Marchitan, N.; Cojocaru, C.; Mereuta, A.; Duca, G.; Cretescu, I.; Gonta, M. Modeling and optimization of tartaric acid reactive extraction from aqueous solutions: A comparison between response surface methodology and artificial neural network. *Sep. Purif. Technol.* **2010**, *75*, 273–285. [CrossRef]
60. Ofoefule, A.U.; Esonye, C.; Onukwuli, O.D.; Nwaeze, E.; Ume, C.S. Modeling and optimization of African pear seed oil esterification and transesterification using artificial neural network and response surface methodology comparative analysis. *Ind. Crop. Prod.* **2019**, *140*, 111707. [CrossRef]
61. Günay, M.E.; Yıldırım, R. Neural network aided design of Pt-Co-Ce/Al_2O_3 catalyst for selective CO oxidation in hydrogen-rich streams. *Chem. Eng. J.* **2008**, *140*, 324–331. [CrossRef]

62. Kumar, S.; Jain, S.; Kumar, H. Process parameter assessment of biodiesel production from a Jatropha–algae oil blend by response surface methodology and artificial neural network. *Energy Sources Part A Recover. Util. Environ. Eff.* **2017**, *39*, 2119–2125. [CrossRef]
63. Maran, J.P.; Priya, B. Comparison of response surface methodology and artificial neural network approach towards efficient ultrasound-assisted biodiesel production from muskmelon oil. *Ultrason. Sonochem.* **2015**, *23*, 192–200. [CrossRef]
64. Aksu, G.; Güzeller, C.O.; Eser, M.T. The Effect of the Normalization Method Used in Different Sample Sizes on the Success of Artificial Neural Network Model. *Int. J. Assess. Tools Educ.* **2019**, *6*, 170–192. [CrossRef]
65. Pham, B.T.; Nguyen, M.D.; Ly, H.-B.; Pham, T.A.; Hoang, V.; Van Le, H.; Le, T.-T.; Nguyen, H.Q.; Bui, G.L. Development of Artificial Neural Networks for Prediction of Compression Coefficient of Soft Soil. In *CIGOS 2019, Innovation for Sustainable Infrastructure*; Ha-Minh, C., Dao, D.V., Benboudjema, F., Derrible, S., Huynh, D.V.K., Tang, A.M., Eds.; Springer: Singapore, 2020.